

Blind Quality Assessment for Slice of Microtomographic Image

Anton Kornilov*[†], Iliia Safonov*[†], Ivan Yakimchuk*

*Schlumberger Moscow Research, Moscow, Russia

[†]National Research Nuclear University MEPhI, Moscow, Russia
kranton94@mail.ru, {isafonov, iyakimchuk}@slb.com

Abstract—The paper considers a new algorithm for blind quality assessment of a slice of X-ray microtomographic image. We selected the following factors impacting on micro-CT image quality with respect to Digital Rock technology: smoothness, sharpness, contrast, absence of high-density regions and ring artifacts. We propose algorithms for estimation of partial quality measures for named factors inside Region-of-Interest, that is in area associated with a sample of rock or granular material. Total quality metrics is calculated as a product of these partial measures. Our method for quality assessment provides reasonable outcomes for synthetic and real slices of micro-CT images. We collected experts' judgments about quality of slices. Proposed solution has a high correlation with scores of experts and outperforms existing blind quality metrics. An application of developed method to all slices allows to obtain quality estimation for 3D micro-CT image.

I. INTRODUCTION

X-ray computed microtomography (micro-CT) [3] is widely used for analysis of various solid and granular materials [4]. Digital Rock is an example analytic technology based on micro-CT data. This technology is applied for estimation of reservoir rocks characteristics in oil and gas industry [1], [2]. Micro-CT “reconstructs” a 3D image of a rock sample from shadow projections. Such digital representation of a core sample enables simulation of its physical and chemical properties. Obviously, the image quality strongly effects on the adequacy and accuracy of such digital model. So far, an operator of micro-CT system made visual quality estimation of reconstructed image. It may lead to selection of non-optimal parameters of scanning and/or reconstruction. Sometimes, micro-CT image can be inapplicable for building a proper digital representation, because its quality is too low. It is preferable to substitute the subjective visual quality assessment by numeric one. The aim of our work is to develop an algorithm and software tool for the quantitative quality assessment of a microtomographic image.

The main challenge of creation of technique for image quality assessment is transformation of subjective knowledge, experience and intuition of experimenters to objective numeric scale. Quality is a vague notion. How to formalize it quantitatively? Are there universal criteria for any type of image or distinct measures for limited subset of images? That is why, image quality assessment (IQA) is one of the hottest problems in image and video processing. The no-reference

(blind or unsupervised) IQA methods are intended for assessing the quality of an image with no prior information about its reference pristine version. Despite huge efforts, so far there are no commonly adopted blind quality metrics intended for any type of image affected by several types of various defects [5].

The majority of existing quality measures is aimed with conventional photo of natural scenes. In the best of our knowledge, there are no numerical quality metrics intended for assessment of X-ray micro-CT images in a prior art. Quality of micro-CT image depends on many factors. Part of them are general for any images, e.g. noise, blur, brightness and contrast. Other factors are specific for computed tomography, e.g. beam hardening, a partial volume effect, the ring artifacts [6]. Some artefacts act approximately equal across a slice. Others have a local nature. As a rule, several causes of quality impairing effect simultaneously. Building of blind quality metric of micro-CT image considering joint action of global and local influential factors is even more challenging in comparison with quality assessment of a conventional photo.

An operator of micro-CT should have possibility for rapid quality assessment to decide re-scan or re-reconstruct image. Sometimes third-parties laboratories perform scanning. In that case, a customer should have a tool for fast quality evaluation of ordered images. Therefore, procedure for quality estimation should process an image in several minutes. Typical micro-CT image has size about 4000×4000×2000 voxels and bit depth 8 or 16 bits per voxel. High computing power and huge memory are required to handle with such image. We decided to assess quality for slices of micro-CT image, because it is way for obtaining a fast solution by means of concurrent processing and an application of existing optimized libraries for processing of 2D images. Quality metrics for whole 3D image can be calculated based on measures of all slices. In the paper we propose new algorithm for blind quality assessment of a slice of micro-CT image.

This paper is organized as follows: in Section II we describe existing blind quality assessment methods; in Section III we propose new algorithm for blind quality assessment of a slice of X-ray microtomographic image; in Section IV we show results of testing proposed method on synthetic images, real Micro-CT images with different exposure and present comparison of assessments by our method and existing blind quality assessment methods with experts' judgments; and in

Section V we conclude on the applicability of the proposed method to assess the quality of micro-CT images.

II. RELATED WORK

Paper [7] presents comprehensive classification of existing blind IQA methods. Quality assessment approaches lie in two main categories: distortion-specific (or partial) and general purpose (or universal). There are numerous publications devoted to various approaches for evaluation of noise level [8], for estimation of image sharpness [9] or blurriness [10], and for assessment of artifacts of lossy compressions. Frequently algorithms for the distortion-specific quality estimation come before correction of corresponding defects, for example, sharpness is assessed for finding of parameters for sharpening, level of JPEG artifacts is estimated for enhancement of compressed images [11]. Majority of the distortion-specific quality measures is intended for idealistic models of distortion, for example additive white Gaussian noise (AWGN) is analyzed only; the metrics are based on assumption of a predominance of considered defects over other one, whereas real images are affected by several distortions jointly. Application of such partial metrics should rely on rigorous analysis of possible defects for given image type and cross-influence of these distortions.

The famous general quality metrics employ machine-learning-based techniques. Almost all existing blind quality assessment methods are “opinion aware”: in the training stage, feature vectors are extracted from the distorted images, then a regression model is learned to map the feature vectors to the associated human subjective scores [12], [13]. The models were trained on images from *Live* dataset [14], that contains 29 pristine images and 779 their copies affected by one from 5 types of distortions (AWGN, JPEG, JPEG2000, Gaussian Blur, Fading). Sometimes the methods apply for training several additional corpuses having similar characteristics, e.g. TID2008 [15].

Blind Image Quality Index (BIQI) [12] implements a two-step approach to assess the quality of photographs. This method is based on usage of features originated from natural scene statistic (NSS) in wavelet domain [16] and assumptions that photos of natural scenes have determined statistic properties, these properties are changed due to distortions, and type and power of distortion can be predicted. First stage of BIQI is classification type of defect. Second one is numerical quality estimation via regression model. Support vector machine (SVM) is used for training classification and regression models. Blind/Referenceless Image Spatial Quality Evaluator (BRISQUE) [13] uses features from NSS in spatial domain [17]. One regression model for all distortions is trained by SVM. Oriented Gradients Image Quality Assessment (OG-IQA) method [18] analyzes correlation of oriented gradients in spatial domain. It was speculated, orientations of local gradients change predictably for distorted photos of natural scenes. One regression model for all distortions is trained by means of Adaptive Boosting algorithm for decision trees. The small number of photos as well as the limited number of deformations in training set lead to low generalization capability of such models.

Natural Image Quality Evaluator (NIQE) [19] does not use distorted image for training. In this method, multivariate Gaussian (MVG) model based on NSS features in spatial domain is calculated for pristine photos only. The quality of the estimated image is estimated as the distance between its MVG and pre-calculated MVG of undistorted photos from *Live* corpus. Integrated Local Natural Image Quality Evaluator (IL-NIQE) [20] algorithm exploits the same idea as NIQE, but IL-NIQE operates with color channels of photo in salient local patches. We suppose, general concept of IL-NIQE can be adjusted for assessment of global quality factors (e.g. noise and blur) of micro-CT images. Surely, MVG model should be trained on representative set of high-quality micro-CT images. However, there are no existing quality metrics considering local specific micro-CT artifacts.

III. ALGORITHM OF QUALITY ASSESSMENT

A. General workflow

There are two approaches for the development of IQA algorithms: deductive (top-down) and inductive (bottom-up) reasoning. Deductive methods are created based on a priori knowledge about characteristics of images and factors impacting on its quality. Outcomes of deductive inference depends on the completeness of the understanding of a problem and the feasibility of making a non-contradicting formal description. Inductive or supervised machine learning algorithms train models based on available dataset. Outcome of machine-learning-based techniques depends primarily on completeness and consistency of the training, testing, and validation sets. It is necessary to collect the representative dataset to provide high generalization capability of trained model. Collection of big and diverse dataset containing micro-CT images is quite difficult and time-consuming problem. So, we decided to formalize experience and intuition of experts about quality of microtomographic image by top-down approach.

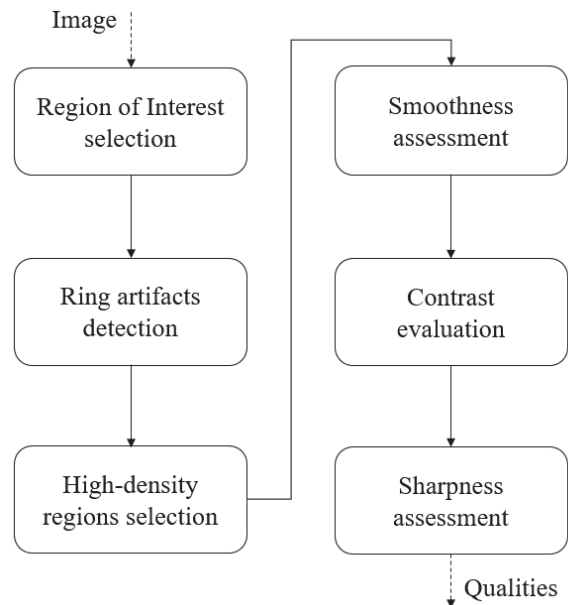


Fig. 1. Workflow for processing of a slice

As a rule, a sample occupies only part of image, so-called Region of Interest (ROI). Quality estimation should be done inside ROI. After literature analysis [3, 5] and discussions with the experts we selected the following main factors that affect the quality of micro-CT images obtained for Digital Rock technology: noise due to short exposure time, noise-like pattern due to insufficient number of shadow projections, blurriness, low contrast, presence of high-density (HD) regions, and ring artifacts. These factors have cross-influence. Nevertheless, our aim is to assess them independently from each other, because sometimes it allows to understand causes of low quality and to give to an operator of micro-CT system the recommendations to improve image quality. We propose to estimate the following five partial quality measures that are dimensionless values in the range from 0 to 1, where 0 corresponds to low quality and 1 corresponds to high quality: Q_n – smoothness; Q_b – sharpness; Q_c – contrast; Q_o – absence of HD regions; and Q_a – absence of ring (or circle) artifacts.

Total quality metrics is combining of these partial measures. If image has low quality due to any factor then corresponding measure should be equal to zero, and total quality measure should be equal to zero too. That is why, reasonable combining of the partial measures is their multiplication:

$$Q = Q_b^{\gamma_b} \times Q_n^{\gamma_n} \times Q_a^{\gamma_a} \times Q_o^{\gamma_o} \times Q_c^{\gamma_c},$$

where Q is total quality metrics for the slice; $\gamma_b, \gamma_n, \gamma_a, \gamma_o$ and γ_c lie in the range $[0, 1]$, and they are used to control of relative importance of the corresponding partial measures, such way for weighting of the multipliers was inspired by structure similarity index (SSIM) [14].

Fig. 1 shows workflow for quality assessment for a slice of microtomographic image. This order of stages is selected intentionally, because each next stage applies information obtained in previous ones. The first stage is ROI selection. All partial measures are estimated for this ROI. Ring artifacts are detected in the second stage. Third stage is detection of HD regions. Smoothness assessment is performed in the fourth stage. The following stages, contrast evaluation and sharpness assessment, use the noise level estimation obtained in smoothness assessment.

B. Region of Interest selection

Intensity range of a slice can vary significantly depending on parameters of micro-CT system and sample, especially in the case of storing an image having 16 bits per voxel. First processing step is intensity normalization of pixels of slice I to the range $[0, 255]$:

$$I(r, c) = \begin{cases} 0 : I(r, c) \leq l, \\ \frac{255(I(r, c) - l)}{(u - l)} : l < I(r, c) < u, \\ 255 : u \leq I(r, c) \end{cases} \quad (1)$$

where (r, c) is the pixel coordinate of the image, $r = 0 \dots N-1$, $c = 0 \dots M-1$, N is the number of rows in the image, M is the

number of columns, l and u are 1 and 95 percentiles calculated from intensity histogram of central part of the slice I .

The algorithm for selection a region associated with a sample searches for a convex region, within which there are distinguishable boundaries between areas of different intensity. It is important to find the areas inside the sample, and there is no need to accurately find the edges of the sample. Often, the noise level in micro-CT images is quite high. Therefore, many well-known filters for detecting boundaries in this case are not applicable, since they will react to noise. In addition, it is not the borders themselves that are of interest, but areas where there are changes in intensity. A variance filter allows to get an image in which relatively large values will be in the pixels, around which there is a change in the intensity of the image areas, and relatively small values in uniform areas. The variance filter [21] is defined as:

$$I_{\text{var}}(r, c) = \frac{1}{W^2} \sum_{i=0}^{W-1} \sum_{j=0}^{W-1} \left(I \left(r + i - \left\lfloor \frac{W}{2} \right\rfloor, c + j - \left\lfloor \frac{W}{2} \right\rfloor \right) - \overline{I}_W(r, c) \right)^2, \quad (2)$$

where $\lfloor \cdot \rfloor$ is the operator of taking the integer part, W is the size of a square window, coordinates (r, c) are changed as: $r = \lfloor W/2 \rfloor \dots N - \lfloor W/2 \rfloor - 1$, $c = \lfloor W/2 \rfloor \dots M - \lfloor W/2 \rfloor - 1$; the expectation of mean value \overline{I}_W within the window is calculated as:

$$\overline{I}_W(r, c) = \frac{1}{W^2} \sum_{i=0}^{W-1} \sum_{j=0}^{W-1} I \left(r + i - \left\lfloor \frac{W}{2} \right\rfloor, c + j - \left\lfloor \frac{W}{2} \right\rfloor \right). \quad (3)$$

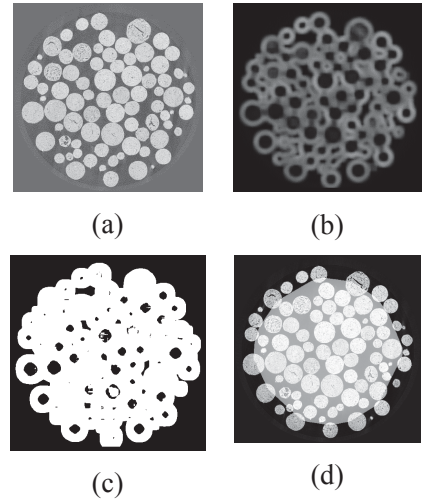


Fig. 2. An illustration of ROI selection steps: (a) initial slice; (b) the result of the variance filter; (c) the result of thresholding for 2b; (d) selected Region of Interest

Fig. 2b shows the result of the variance filter for the image in Fig. 2a. The thresholding of the outcome of variance filter allows to obtain a binary image, in which pixels with values 1 identify that in their local neighborhood the intensity changes. Fig. 2c shows the result of the thresholding. After application of the thresholding several connected regions may be formed. To make them “merge” into a single conglomerate, we use a

morphological closing operation [22]. Several small areas can form near the boundaries of the slice, for example it occurs on the outer border of the holder. To exclude these undesirable areas from consideration, we process further only the convex hull of the largest region. This region extends beyond the sample by approximately half to two thirds of the size of the window of variance filter. To ensure that the entire region is inside the sample, a morphological erosion filter [22] is applied with the size of the structural element equal to the size of the window of variance filter.

As the result of ROI selection, we have binary bitmap ROI , where one means that pixel is inside ROI and zero means that pixel is outside. Area of ROI is calculated as:

$$S_{ROI} = \sum_r \sum_c ROI(r, c).$$

In addition to ROI, we calculate binary mask MSK for excluding pixels equal to 0 (pure black) or $2^n - 1$ (pure white), where n is a bit depth. We assume, that intensities in these pixels were clipped, and we cannot rely on their values. Assessments of smoothness, sharpness and contrast are performed for pixels with coordinate (r, c) for which $MSK(r, c)$ equals 1. Mask MSK is calculated as logical conjunction of ROI and inverted masks for white and black:

$$MSK(r, c) = ROI(r, c) \text{ and } (\text{not } f_w(r, c)) \text{ and } (\text{not } f_b(r, c)),$$

where mask for white is:

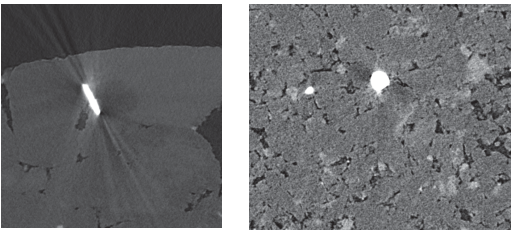
$$f_w(r, c) = \begin{cases} 1: I(r, c) = 2^n - 1 \text{ and } ROI(r, c) = 1, \\ 0: \text{otherwise} \end{cases}$$

where mask for black is:

$$f_b(r, c) = \begin{cases} 1: I(r, c) = 0 \text{ and } ROI(r, c) = 1, \\ 0: \text{otherwise} \end{cases}$$

C. Selection of high-density regions

By high-density (HD) regions, we mean parts of the sample, in which X-ray attenuation is significantly and abruptly different from neighboring parts. The total attenuation of the X-ray intensity is an a priori unknown combination of the photoelectric effect and the Compton effect [3], which cannot be properly accounted in reconstruction model. As a result, such regions often cause distortions in reconstructed images, e.g., fake decrease of attenuation coefficient around edges of HD particles Fig. 3b, strikes Fig. 3a.



(a)

(b)

Fig. 3. Examples of high-density regions

Such distortions lead to errors in image segmentation as well as in smoothness and sharpness assessments. The larger the area of HD regions the stronger the negative impact on quality. Percentage of pixels in ROI related to HD regions serves as a parameter for quality characterization:

$$P_{HD} = 100 \frac{\sum_r \sum_c f_{HD}(r, c)}{S_{ROI}},$$

where indicator function f_{HD} for HD pixels selection is:

$$f_{HD}(r, c) = \begin{cases} 1: I(r, c) \geq T_{HD} \text{ and } ROI(r, c) = 1, \\ 0: \text{otherwise} \end{cases},$$

where threshold T_{HD} is calculated as:

$$T_{HD} = \min \left(c \left(\max \left\{ i \left| \sum_{k=i}^{2^n-1} H_{ROI}[k] \geq S_{ROI} P_W \right\} + 2^n - 1 \right), \left(2^n - 1 \right) \right),$$

where c is a coefficient less 1, H_{ROI} is histogram of intensity of pixels belonging in ROI, percentage of pure white pixels inside ROI P_W calculated as:

$$P_W = 100 \frac{\sum_r \sum_c f_w(r, c)}{S_{ROI}}.$$

Quality measure Q_o characterizing of absence of high-density regions is calculated as:

$$Q_o = \frac{1}{P_{HD} + 1}.$$

D. Smoothness assessment

Existing methods for noise level estimation works reasonable for a limited type of noises only. As a rule, the method is capable to do assessment for additive or multiplicative white Gaussian noises (AWGN or MWGN) [8]. In case of micro-CT images, we have mixture of several types of correlated noises and defects of reconstructions, that look like noise.

First step of smoothness assessment is intensity normalization for the image according to statement (1), where l and u are minimal and maximal intensities in the central part of the slice. We assume, standard deviation for uniform area of mineral matrix can be used for noise level estimation. Smoothness is inverse value for noise level. Variance filter (see statements (2) and (3)) serves for calculation of local standard deviations and means. Estimation should be done only in local windows, for which majority of pixels for corresponding window in MSK equals to one. We calculate two arrays, STD and MN , as follows:

$$\left\{ STD(t_1) = \sqrt{I_{\text{var}}(r, c)}, MN(t_1) = \overline{I}_W(r, c) \mid p_1 \leq S_{MSK} \right\},$$

where p_1 is allowable percentage of masked pixels inside current local window, where percentage of masked pixels S_{MSK} is calculated as:

$$S_{MSK} = \frac{1}{W^2} \sum_{i=0}^{W-1} \sum_{j=0}^{W-1} MSK \left(r+i - \left\lfloor \frac{W}{2} \right\rfloor, c+j - \left\lfloor \frac{W}{2} \right\rfloor \right),$$

where $r = \lceil W/2 \rceil \dots N - \lceil W/2 \rceil - 1$, $c = \lceil W/2 \rceil \dots M - \lceil W/2 \rceil - 1$ and W is a size of the local window.

We wish to do assessment for lighter areas of mineral, not darker areas of voids. For this purpose, we drop p_2 percent of darker blocks:

$$\left\{ STD(t_2) = STD(t_1), MN(t_2) = MN(t_1) \mid T_{MM} \leq MN(t_1) \right\},$$

where t_2 is sequential index, T_{MM} is p_2 percentile for array MN .

Noise level NL is estimated as mean value among p_3 percent of the least standard deviations in the array STD . We calculate smoothness Q_n as:

$$Q_n = 1 - \left(\max \left(0, \frac{\min(NL - LNL, HNL - LNL)}{HNL - LNL} \right) \right)^2,$$

where LNL is the biggest standard deviation, which we consider corresponding to low noise level; HNL the smallest standard deviation, which we consider corresponding to ultimately high noise level, when processing of such image is meaningless.

E. Contrast evaluation

Contrast can be estimated as “width of histogram” that is the difference between the lightest and the darkest areas masked by MSK . To exclude bias due to presence of various artifacts, for example bright rays from HD regions, it is preferable to estimate contrast as difference between 95 and 5 percentiles of intensities of those pixels that corresponds to one in mask MSK . However, width of histogram depends on noise level. Higher noise leads to spreading of histogram that leads to contrast overestimation. Because adding of noise leads to histogram extending, we assumed, that inverse operation that is noise suppression will lead to histogram narrowing. Indeed, it takes place. Box filter is the fastest one for noise suppression. We suggest setting up size of convolution kernel of box filter depending on noise level. So, the filtering allows to make contrast assessment almost irrespectively to noise level. Noise filtering is performed by Box filter and consists in convolution of the slice with square kernel:

$$I_b = K * I,$$

where symbol $*$ denotes convolution.

Quality measure of contrast Q_c is calculated as:

$$Q_c = \frac{\max(I_{b95} - I_{b05}, HC)}{HC},$$

where I_{b05} and I_{b95} are 5 and 95 percentiles accordingly of intensities of those pixels from I_b that corresponds to one in mask MSK , HC is the least difference between 95 and 5 percentiles, which is estimated by the expert as good enough for further processing.

F. Sharpness assessment

There is no commonly accepted blurriness or sharpness measure. Existing approaches can make robust estimation for images affected by isotropic Gaussian blur only [10]. In the case of micro-CT images, we have much more complex model of blurring. Moreover, blurring almost always is accompanied by noise. It is well-known a human estimates noisy image as a sharper. Our intention is estimation of sharpness independently from other factors of quality. Thus, beforehand we should suppress noise. However, box-filter is inapplicable in this case, because it leads to blurring of edges; it is preferable to apply edge-preserving filter, for example bilateral filter [23].

First step of sharpness assessment is intensity normalization for the slice according to statement (1) where l and u are minimal and maximal intensities of central part of the slice. After intensity normalization we apply bilateral filter several times depending on noise level. The bilateral filter is defined as:

$$I_f(r, c) = \frac{\sum_{i=-S/2}^{S/2} \sum_{j=-S/2}^{S/2} I(r+i, c+j) \times v(i, j) \times w(I(r+i, c+j) - I(r, c))}{\sum_{i=-S/2}^{S/2} \sum_{j=-S/2}^{S/2} v(i, j) \times w(I(r+i, c+j) - I(r, c))},$$

$$v(i, j) = \exp\left(-\frac{i^2 + j^2}{2\sigma_D^2}\right),$$

$$w(x) = \exp\left(-\frac{x^2}{2\sigma_R^2}\right),$$

where σ_D and σ_R are smoothing parameters, S is a filter size.

Sharpness quality metrics Q_b is calculated based on Crete' blurriness metrics [10]. The main assumption of the metrics is the following: there is small difference between blurred image and its re-blurred copy. Estimation is performed in masked by MSK regions. We compare responses of high-pass filter of initial image I and its re-blurred copy B . To be able to detect blurring by motion blur we consider re-blurring in vertical and horizontal directions separately:

$$B_v = K_l * I_f,$$

$$B_h = K_l^T * I_f,$$

where K_l is convolution kernel 1 by n of low-pass filter, for instance $K_l = [1\ 1\ 1\ 1\ 1\ 1\ 1\ 1\ 1\ 1]/9$. The next step is an obtaining of gradients by high-pass filtering and getting of absolute values for image I and its re-blurred copies. The step is performed separately in vertical and horizontal directions too.

$$dI'_v = |K_h * I_f|, dI'_h = |K_h^T * I_f|,$$

$$dB'_v = |K_h * B_v|, dB'_h = |K_h^T * B_h|,$$

where K_h is convolution kernel 1 by m of high-pass filter, for instance $K_h = [1\ -1]$.

We take into account pixels of interest by multiplication of corresponding pixels of gradient images and MSK :

$$dI_v(r, c) = dI'_v(r, c) \times MSK(r, c),$$

$$dI_h(r, c) = dI'_h(r, c) \times MSK(r, c),$$

$$dB_v(r, c) = dB'_v(r, c) \times MSK(r, c),$$

$$dB_h(r, c) = dB'_h(r, c) \times MSK(r, c).$$

Differences between gradients of image I_f and re-blurred copies are calculated as following:

$$dV_v(r, c) = \max(0, dI_v(r, c) - dB_v(r, c)),$$

$$dV_h(r, c) = \max(0, dI_h(r, c) - dB_h(r, c)).$$

Then we calculate the sums of vertical and horizontal gradients as well as the sums of differences between gradients:

$$sI_v = \sum_r \sum_c dI_v(r, c), sI_h = \sum_r \sum_c dI_h(r, c),$$

$$sV_v = \sum_r \sum_c dV_v(r, c), sV_h = \sum_r \sum_c dV_h(r, c).$$

Sharpness Q_b for the slice is calculated as:

$$Q_b = \min \left(1, c_1 \cdot \max \left(0, 1 - \max \left(\frac{sI_v - sV_v}{sI_v}, \frac{sI_h - sV_h}{sI_h} \right) - c_2 \right) \right),$$

where c_1 and c_2 are constants.

G. Detection of ring artifacts

There are several electronic defects in micro-CT deteriorating the image and, in most cases, destroying it. The most famous such defect is the failure of a detector pixels, which results in prominent ring artifacts [3]. As the X-ray source and the detector array are tightly joined at the sampling unit, the failure of an individual detector element or the corresponding processing channel respectively becomes specifically visible. During the filtered shadow projections, the virtual lines connecting the corresponding corrupted detector element and the X-ray source, which sometimes are called defective beams, form the tangents of a circle. This means that all values outside the circle are seriously concerned by this

artifact. Inconsistencies with the measured values of the corresponding other projection directions in fact arise for each point of each line. Several approaches for mitigation of ring artifacts were developed by manufacturers of micro-CT systems, for example: random movement between acquisitions of adjacent shadow projections, post-processing of shadow projections before reconstructions. Combination of these approaches allows to suppress majority of ring artifacts. Nevertheless, part of ring artifacts remains and deteriorates reconstructed image significantly.

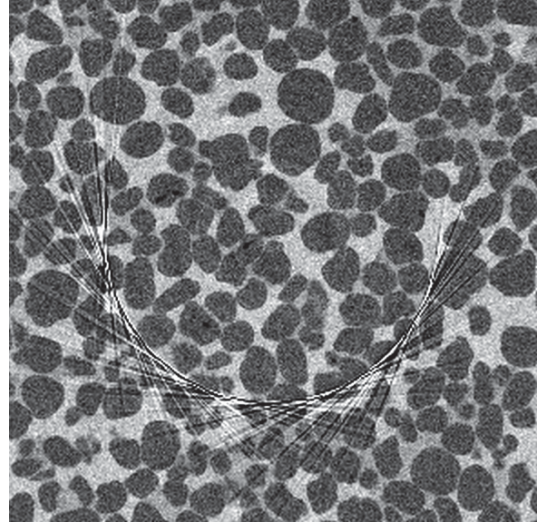


Fig. 4. Example (in inverted colors) of image fragment deteriorated by ring artifacts

Fig. 4 shows example of strong ring artifacts. First step of ring artifacts detection is intensity normalization for the image according to statement (1). Then we transform the slice to polar coordinate system, where origin is in the center of initial slice (see Fig. 5a). In polar coordinate system rings around the center of the slice are transformed to the vertical lines. Application of matched filter allows to emphasize such lines. We use matched filter with convolution kernel having the following identical 31 rows:

$$[-1\ -1\ -1\ -1\ 2\ 2\ 2\ 2\ -1\ -1\ -1\ -1].$$

Fig. 5b also shows outcome of matched. Thresholding of the outcome of matched filter selects pixels of rings. To consider ROI, the result of thresholding is multiplied by image ROI. Then morphological dilation with vertically-oriented structure element is used to merge neighboring regions. Finally, we make labelling of connected regions and eliminate regions, which have bounding box sizes that are not satisfied to predefined rules. Quality measure Q_a characterizing of absence of ring artifacts is calculated as:

$$Q_a = \min \left(1 - \frac{100S_{rings}}{S_{ROI}}, 0 \right).$$

where area S_{rings} is sum of pixels of all survived regions satisfying to predefined rules.

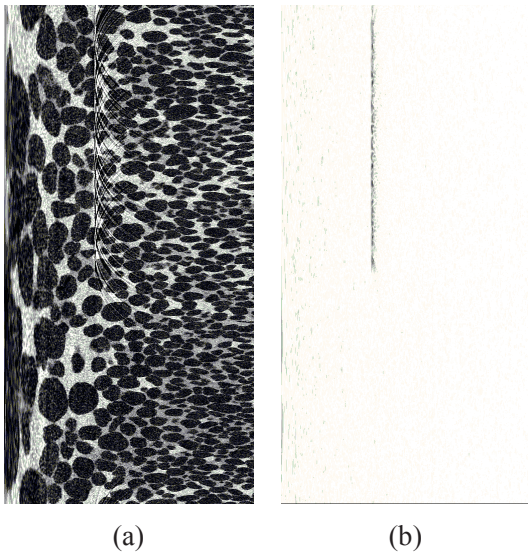


Fig. 5. Cropped slice with ring artifact in polar coordinates (a) and outcome of matched filter with founded artifact (b)

IV. RESULTS

A. Outcomes for synthetic image

Our intention is development of quality metrics which are capable to estimate several quality factors independently from each other. We propose synthetic image (see Fig. 6a) that allows controlling of blurriness, noise level and contrast independently from each other. Our algorithms for calculation of quality metrics for smoothness, contrast and sharpness provide expected reasonable outcomes (see Fig. 6b for smoothness, Fig. 6c for sharpness and Fig. 6d for contrast): each partial quality measure falls down with growing of power of corresponding defect almost irrespectively to other defects.

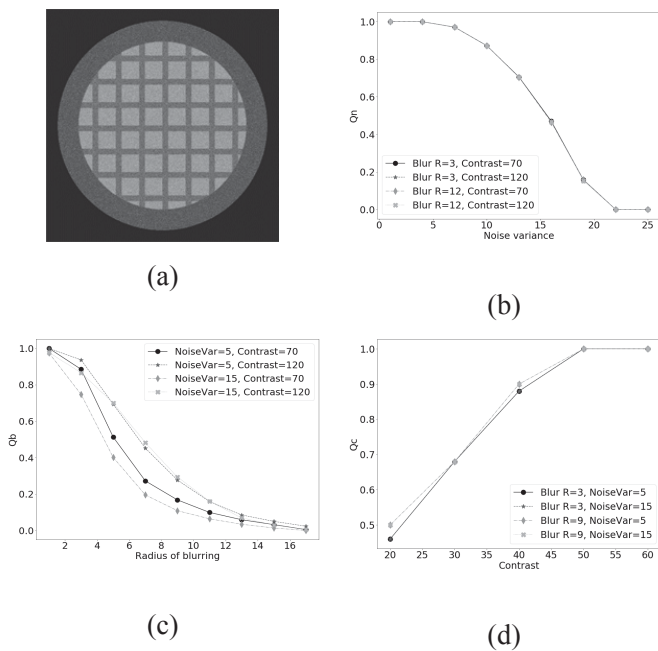


Fig. 6. Synthetic image (a); smoothness (b), sharpness (c) and contrast (d) depending on defect power for synthetic image

B. Micro-CT images with different exposure

We scanned the same sample 6 times with different exposure time and number of frames for averaging. A longer exposure time and a greater number of frames for averaging allow to obtain high-quality image. A shorter exposure time and absence of averaging corresponds to noisy image (see example of two images in Fig. 7). Actually, smoothness metrics goes down with increasing of noise level with our method (see Table I) and other quality measures are approximately the same, as we expected.

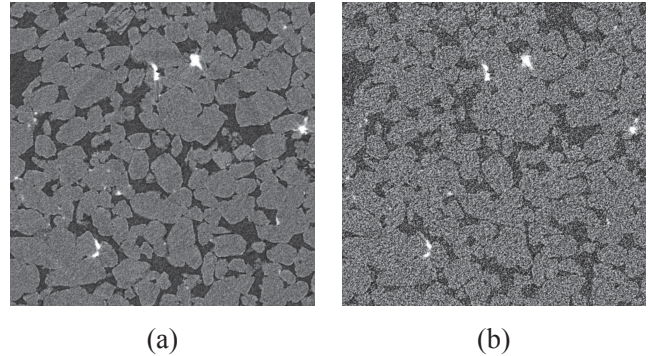


Fig. 7. Example of images different exposure: (a) Exp. Time 1 s, 11 frames; (b) Exp. Time 0.7 s, 1 frame

TABLE I. SMOOTHNESS ASSESSMENT

Image	Exp. time, s	1	1	1	0.7	0.3	0.1
	Frames num.	11	3	1	1	1	1
Smoothness, Q_n		1.0	0.97	0.87	0.83	0.65	0.0

C. Comparison with experts' scores

Based on pairwise comparison method [24] we converted experts' judgments about quality of 10 images to continuous scale and compare with assessments produced by our algorithm. We asked three experts to compare 10 slices of the same sample scanned by various micro-CT systems in different modes. The experts compared sharpness, smoothness, and total quality for pairs of images. Fig. 8 shows two images from our test set. Plots in Fig. 9, Fig. 10 and Fig. 11 demonstrates high correlation between assessments by our algorithm and experts. Table II contains Mean Absolute Difference (MAD) for Q_n (smoothness), Q_b (sharpness), and Q (total quality) between assessments by our algorithm and experts. MAD is quite small.

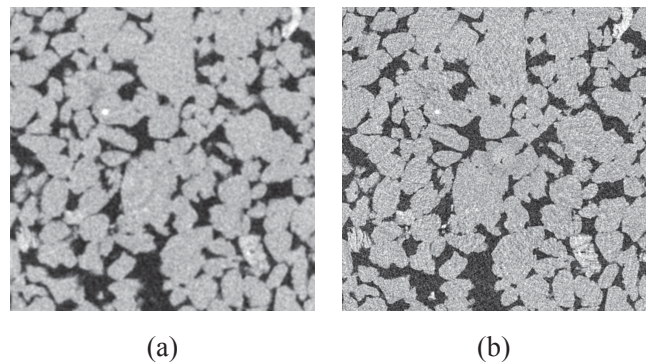


Fig. 8. Examples of two images from test set: (a) 2nd image; (b) 5th image

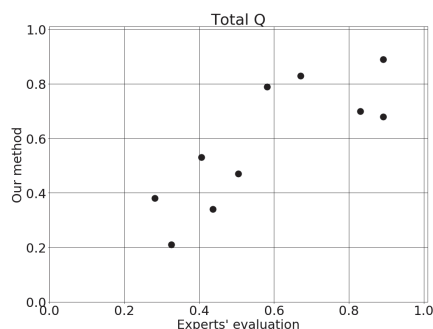


Fig. 9. Comparison of assessments of total quality by our method and experts'

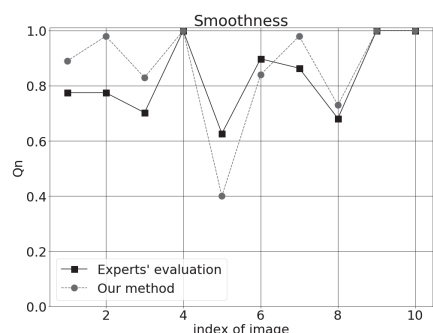


Fig. 10. Comparison of assessments of smoothness by our method and experts'

Table III contains MAD for image quality between assessments by the experts and our algorithm, as well as the existing blind quality metrics. Some of existing metrics (in particular BIQI and IL-NIQE) have good correlation with experts' opinion. However, those measures cannot estimate presence of specific micro-CT artifacts such as HD regions and rings. For assessment of micro-CT images our solution outperforms existing blind image quality metrics.

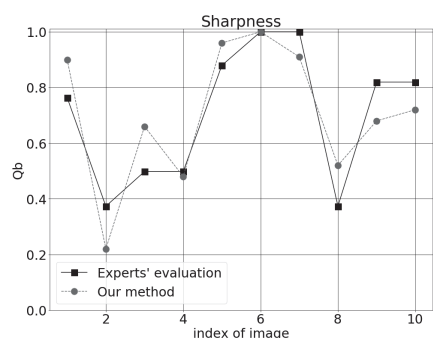


Fig. 11. Comparison of assessments of sharpness by our method and experts'

TABLE II. MAD BETWEEN ASSESSMENTS BY OUR METHOD AND EXPERTS'

Measure	MAD
Q_n	0.09
Q_b	0.10
Q	0.12

TABLE III. MAD BETWEEN ASSESSMENTS BY METHODS AND EXPERTS'

Method	MAD
Our method	0.12
BIQI [12]	0.16
BRISQUE [13]	0.24
NIQE [19]	0.30
IL-NIQE [20]	0.16
OG-IQA [18]	0.21

We implemented our algorithm in multi-platform application on C++ programming language. Processing time of one slice with size 4000 by 4000 pixels is about 3 s on PC with CPU Intel Core I7-5600 2.6 GHz. We expect to achieve total processing time of whole 3D micro-CT image about 10-15 minutes thanks to concurrency.

V. CONCLUSION

We proposed no-reference metrics for assessment of quality of a slice of micro-CT image. It was done based on rigorous analysis of factors influenced on visual quality of microtomographic images. The metrics is calculated as product of the following partial quality measures: smoothness, sharpness, contrast, absence of high-density regions, and absence of ring artifacts. Proposed partial measures and total quality metrics have high correlation with scores given by experts in experiment based on pairwise comparison. Also, our algorithm outperforms several well-known blind quality metrics. Implemented in C++, the processing is fast and takes about 3 s for one microtomographic slice. An application of developed method to all slices allows to obtain quality assessment for 3D micro-CT image.

REFERENCES

- [1] C.F. Berg, O. Lopez, and H. Berland, "Industrial applications of digital rock technology", *Journal of Petroleum Science and Engineering*, vol. 157, 2017, pp. 131-147.
- [2] D.A. Koroteev, O. Dinariev, N. Evseev, D.V. Klemm, S. Safonov, O.M. Gurpinar, S. Berg, C. van Kruijsdijk, M. Myers, L.A. Hathon, H. de Jong, and R. Armstrong, "Application of digital rock technology for chemical EOR screening", in *Proc. SPE Enhanced Oil Recovery Conf.*, Jul. 2013, pp. 1-12.
- [3] T.M. Buzug, *Computed tomography: from photon statistics to modern cone-beam CT*. New York: Springer Science & Business Media, 2008.
- [4] I. Safonov, I. Yakimchuk, and V. Abashkin, "Algorithms for 3D Particles Characterization Using X-Ray Microtomography in Proppant Crush Test", *Journal of Imaging*, vol. 4(11), 2018, pp. 134.
- [5] Y. Ding, *Visual Quality Assessment for Natural and Medical Image*. Springer Berlin Heidelberg, 2018.
- [6] J.F. Barrett, and N. Keat, "Artifacts in CT: recognition and avoidance", *Radiographics*, vol. 24(6), 2004, pp. 1679-1691.
- [7] M. Jenadeh, M.M. Masaeh, and M.E. Moghaddam, "Blind image quality assessment based on aesthetic and statistical quality-aware features", *Journal of Electronic Imaging*, vol. 26(4), 2017, pp. 043018.
- [8] S. Pyatykh, J. Hesser, and L. Zheng, "Image noise level estimation by principal component analysis", *IEEE transactions on image processing*, vol. 22(2), 2013, pp. 687-699.
- [9] I.V. Safonov, M.N. Rychagov, K. Kang, and S.H. Kim, "Adaptive sharpening of photos", *Color Imaging XIII: Processing, Hardcopy, and Applications. International Society for Optics and Photonics*, vol. 6807, 2008, pp. 68070U.

- [10] F. Crete, T. Dolmiere, P. Ladret, and M. Nicolas, "The blur effect: perception and estimation with a new no-reference perceptual blur metric", *Human vision and electronic imaging*, vol. 6492, 2007, pp. 649201.
- [11] I.V. Safonov, I.V. Kurilin, M.N. Rychagov, and E.V. Tolstaya, *Adaptive Image Processing Algorithms for Printing*. Springer Singapore, 2018.
- [12] A.K. Moorthy, and A.C. Bovik, "A two-step framework for constructing blind image quality indices", *IEEE Signal processing letters*, vol. 17(5), 2010, pp. 513-516.
- [13] A. Mittal, A.K. Moorthy, and A.C. Bovik, "No-reference image quality assessment in the spatial domain", *IEEE Transactions on Image Processing*, vol. 21(12), 2012, pp. 4695-4708.
- [14] H.R. Sheikh, M.F. Sabir, and A.C. Bovik, "A statistical evaluation of recent full reference image quality assessment algorithms", *IEEE Transactions on Image Processing*, vol. 15(11), 2006, pp. 3440-3451.
- [15] N. Ponomarenko, V. Lukin, A. Zelensky, K. Egiazarian, M. Carli, and F. Battisti, "TID2008-a database for evaluation of full-reference visual quality assessment metrics", *Advances of Modern Radioelectronics*, vol. 10(4), 2009, pp. 30-45.
- [16] A. Srivastava, A.B. Lee, E.P. Simoncelli, and S.C. Zhu, "On advances in statistical modeling of natural images", *Journal of mathematical imaging and vision*, vol. 18(1), 2003, pp. 17-33.
- [17] D.L. Ruderman, and W. Bialek, "Statistics of natural images: Scaling in the woods", *Advances in neural information processing systems*, 1994, pp. 551-558.
- [18] L. Liu, Y. Hua, Q. Zhao, H. Huang, and A.C. Bovik, "Blind image quality assessment by relative gradient statistics and adaboosting neural network", *Signal Processing: Image Communication*, vol. 40, 2016, pp. 1-15.
- [19] A. Mittal, R. Soundararajan, and A.C. Bovik, "Making a "completely blind" image quality analyser", *IEEE Signal Processing Letters*, vol. 20(3), 2013, pp. 209-212.
- [20] L. Zhang, L. Zhang, and A.C. Bovik, "A feature-enriched completely blind image quality evaluator", *IEEE Transactions on Image Processing*, vol 24(8), 2015, pp. 2579-2591.
- [21] A. Fabijańska, "Variance filter for edge detection and edge-based image segmentation", in *Proc. IEEE Conference on Perspective Technologies and Methods in MEMS Design (MEMSTECH)*, 2011, pp. 151-154.
- [22] P. Soille, *Morphological image analysis: principles and applications*. New York: Springer Science & Business Media, 2013.
- [23] C. Tomasi, and R. Manduchi, "Bilateral filtering for gray and color images", *Sixth International Conference on Computer Vision*, Jan.1998, pp. 839-846.
- [24] R.K. Mantiuk, A. Tomaszewska, and R. Mantiuk, "Comparison of four subjective methods for image quality assessment", *Computer Graphics Forum*, vol. 31(8), 2012, pp. 2478-2491.